International Journal of Solids and Structures 49 (2012) 3605–3615

Contents lists available at SciVerse ScienceDirect

International Journal of Solids and Structures

journal homepage: www.elsevier.com/locate/ijsolstr

New ductile fracture criterion for prediction of fracture forming limit diagrams of sheet metals

Yanshan Lou, Hoon Huh *, Sungjun Lim, Keunhwan Pack

School of Mechanical, Aerospace and Systems Engineering, KAIST, 335, Gwahangno, Daeduk Science Town, Daejeon 305-701, South Korea

ARTICLE INFO

Article history:
Available online 6 March 2012

Keywords:
Ductile fracture criterion
Fracture forming limit diagram
Fracture locus
Shear fracture
Sheet metal forming

ABSTRACT

A ductile fracture criterion is newly proposed to model fracture behavior of sheet metals for nucleation, growth and shear coalescence of voids during plastic deformation. In the new ductile fracture criterion, void nucleation is described as a function of the equivalent plastic strain, void growth is a function of the stress triaxiality and void coalescence is controlled by the normalized maximal shear stress. The new ductile fracture criterion is applied to construct a fracture forming limit diagram (FFLD) of a dual phase steel sheets of DP780 (1.0t). The FFLD is approximated using both the reverse engineering method and circle grid analysis (CGA) since DP780 fails with slight thickness reduction from the analysis of the fracture surface. Predicted FFLDs are compared to experimental results to validate the performance of the new criterion in the intermediate stress triaxiality between 1/3 and 2/3. The new criterion is also applied to construct the fracture locus of Al 2024-T351 (Bao and Wierzbicki, 2004) to validate the performance of the new criterion in the low and negative stress triaxiality. The fracture locus constructed by the new criterion are close to the experimental data points for all these two materials in a wide stress range from the uniaxial compression to the balanced biaxial tension. The new ductile fracture criterion is recommended to be utilized in finite element analysis to predict the onset of ductile fracture of sheet metals.

1. Introduction

Forming limit diagrams (FLD) have been widely used to predict the formability in sheet metal forming processes since FLDs were proposed by Keeler and Backofen (1963) and Goodwin (1968). FLDs can be constructed by experiments such as hemispherical punch-stretch tests and Marciniak cup tests (Marciniak et al., 1973). These experimental methods, however, require intensive efforts and tremendous time. For more efficient construction of FLDs, many analytical models were proposed such as Hill's localized necking model (Hill, 1952), Swift's diffuse necking model (Swift, 1952), the Marciniak–Kuczynski model (M–K model) (Marciniak and Kuczynski, 1967), the Vertex theory (Stören and Rice, 1975; Zhu et al., 2001), the modified maximum force criterion (MMFC) (Hora et al., 1996). The analytical models reviewed above are mainly applied to predict formability of sheet metals based on necking or thickness reduction. Consequently, failure cannot be estimated by these models in low or negative stress triaxiality where there is no or negligible thickness reduction.

Metals and alloys usually fail as the result of nucleation, growth and coalescence of microscopic voids. Nucleation of voids was investigated and modeled by Argon et al. (1975), Goods and Brown (1979) and Gurson (1977). Rice and Tracey (1969) modeled the growth of a single spherical void in an infinite solid. McClintock (1968) analytically described the growth of voids with a cylindrical shape. Coalescence of voids was experimentally investigated by Weck and Wilkinson (2008) using model materials.

Based on tremendous experimental observation and analytical studies of nucleation, growth and coalescence of voids, dozens of ductile fracture criteria were also proposed which could be used to predict forming limits in low and negative stress triaxiality (Cockcroft and Latham, 1968; Brozzo et al., 1972; Oh et al., 1979; Oyane et al., 1980; Clift et al., 1990; Ko et al., 2007). The forming limits predicted by ductile fracture criteria are named as fracture forming limit diagrams (FFLD) which present forming limits in the space of $(\varepsilon_2, \varepsilon_1)$ from the uniaxial compression to the balanced biaxial tension.

Many research works (Takuda et al., 1999a,b, 2000; Han and Kim, 2003; Ozturk and Lee, 2004; Liu et al., 2009; Chen et al., 2010; Lou et al., 2010a,b) have been carried out to verify the applicability of ductile fracture criteria to predict the formability of sheet metals. However, the stress triaxiality of these applications is limited to its range between 1/3 and 2/3 which ranges from the uniaxial tension to the balanced biaxial tension, respectively. Formability in the low and negative stress triaxiality $(-1/3 < \eta < 1/3)$ has not been comprehensively studied until a series of tests were conducted by Bao and Wierzbicki (2004). These

* Corresponding author. Tel.: +82 42 350 3222; fax: +82 42 350 3210.
E-mail address: hhuh@kaist.ac.kr (H. Huh).

0020-7683/$ - see front matter © 2012 Elsevier Ltd. All rights reserved.
doi:10.1016/j.ijsolstr.2012.02.016

Nomenclature

ε_1, ε_2	two principal strains in plane stress conditions, $\varepsilon_1 \geqslant \varepsilon_2$
$\bar{\varepsilon}$, $\bar{\varepsilon}_f$	equivalent plastic strain and equivalent plastic strain to fracture
$\bar{\varepsilon}_{t0}, \bar{\varepsilon}_{p0}, \bar{\varepsilon}_{b0}, \bar{\varepsilon}_{s0}$	equivalent plastic strain to fracture in the uniaxial tension, plane strain, balanced biaxial tension and pure shear conditions, respectively
β	strain path, $\beta = d\varepsilon_2/d\varepsilon_1$
σ_1, σ_2, σ_3	three principal stresses, $\sigma_1 \geqslant \sigma_2 \geqslant \sigma_3$
s_1, s_2, s_3	three deviatoric principal stresses, $s_1 \geqslant s_2 \geqslant s_3$
σ_m	mean or hydrostatic stress, $\sigma_m = (\sigma_1 + \sigma_2 + \sigma_3)/3$
$\bar{\sigma}$ or σ_e	equivalent stress
$\tau_{\max}$	maximal shear stress
η	stress triaxiality, $\eta = \sigma_m/\bar{\sigma}$
$\theta, \bar{\theta}$	Lode angle and Lode angle parameter
L	Lode parameter, $L = (2\sigma_2 - \sigma_1 - \sigma_3)/(\sigma_1 - \sigma_3)$
K, ε_0, n	coefficients in the Swift strain hardening model
C_1, C_2, C_3	material constants in the new ductile fracture criterion
D_n, D_g, D_c	damage accumulation caused by nucleation, growth and coalescence of voids, respectively

tests included upsetting tests, shear tests and tensile tests of Al 2024-T351. The test results provided clues to fracture strain for a wide range of the stress triaxiality. Since then, shear fracture in the low and negative stress triaxiality attracted increasing attention and effort. Bao and Wierzbicki (2004) proposed a fracture locus with dependence on the stress triaxiality. Bai and Wierzbicki (2008) developed an asymmetric fracture model in the space of the equivalent plastic strain to fracture, the stress triaxiality and the Lode angle parameter. Wierzbicki et al. (2005) evaluated seven fracture models based on the experimental results of Al 2024-T351. Xue (2008) incorporated void shearing damage effect in the Gurson–Tvergaard–Needleman model (Gurson, 1977; Tvergaard and Needleman, 1984). Bai and Wierzbicki (2010) transformed the Mohr–Coulomb criterion to construct the fracture locus in the space of the equivalent plastic strain to fracture, the stress triaxiality and the Lode angle parameter by combining the Mohr–Coulomb criterion with a new hardening rule with pressure and Lode angle dependence. Li et al. (2010) applied the modified Mohr–Coulomb criterion to predict shear-induced fracture in sheet metal forming. Ductile fracture criteria developed recently are based on the assumption that the equivalent plastic strain to fracture depends on the stress triaxiality and the Lode angle parameter. Effect of the stress triaxiality was studied extensively on nucleation and growth of voids (Rice and Tracey, 1969; Brozzo et al., 1972; Oyane et al., 1980; Gurson, 1977; Tvergaard and Needleman, 1984). The role of the Lode angle parameter and its physical mechanisms, however, remain unclear (Li et al., 2011). Another limitation of ductile fracture criteria proposed above is that the cut-off value of the stress triaxiality is not correctly modeled which was reported to be important in high velocity impact simulation (Teng and Wierzbicki, 2006).

In this paper, nucleation, growth and coalescence of voids are analyzed comprehensively to develop reasonable models to describe these processes. These models are combined to construct a new ductile fracture criterion. Parametric study is carried out to investigate the effect of the normalized maximum shear stress and the stress triaxialility on the shape of FFLDs. The new criterion is applied to construct the FFLD of DP780 as well as the fracture locus of Al 2024-T351 to validate their performance on prediction of the equivalent plastic strain to fracture in a wide range of stress states from the uniaxial compression to the balanced biaxial tension of sheet metals.

2. Development of a new ductile fracture criterion

2.1. Microscopic analysis of ductile fracture

In the microscopic viewpoint, ductile fracture is preceded by severe plastic deformation involving nucleation, growth and coalescence of voids in metals and alloys. These three mechanisms will be carefully analyzed and proper models will be selected and proposed in this section.

2.1.1. Nucleation of voids

Void nucleation initiates at interfaces of inclusions and second phase particles with plastic deformation. A number of models have been proposed to explain the mechanism of void nucleation. Normally these models involve a critical debonding stress between material matrices and inclusions or second phase particles (Argon et al., 1975; Goods and Brown, 1979). With these stress-based nucleation criteria, there is no macroscopic tension force to debond interfaces of inclusions or second phase particles in upsetting tests with a stress triaxiality of about $-1/3$. Moreover, a negative stress triaxiality suppresses the growth of voids as explained in the following section. Consequently, ductile fracture cannot be estimated in upsetting tests if nucleation of voids is modeled as a function of the critical debonding stress, which conflicts with experimental observation of ductile fracture in upsetting tests with a negative hydrostatic stress (Bao and Wierzbicki, 2004; Li et al., 2011). Alternatively, Gurson (1977) proposed a strain controlled nucleation model which says that the rate of void nucleation is a function of the equivalent plastic strain. With a strain-based nucleation model, voids nucleate when metals deforms plastically at the grain boundary due to existence of the microscopic tensile force though the macroscopic mean stress is negative. These processes increase the number and density of voids. With strain-based nucleation models, the nucleation of voids can be reasonably described in upsetting tests. From the analysis above, strain-based nucleation models are more reasonable than stress-based nucleation ones for the macroscopic modeling of ductile fracture. Consequently, void nucleation is modeled as a function of the equivalent plastic strain as below:

$$D_n = D_n(\bar{\varepsilon}) \tag{1}$$

Here the number of voids nucleated is assumed to be a function the equivalent plastic strain.

2.1.2. Growth of voids

Void growth is mainly influenced by the mean stress σ_m according the experimental observation (McClintock, 1968; Li et al., 2011). High mean stress accelerates void growth while negative mean stress suppresses void growth, thereby delaying fracture (Hosford and Caddell, 1983). Void growth has been described by numerous mathematical models such as the Rice–Tracey (Rice and Tracey, 1969) and the McClintock criteria (McClintock, 1968) with the influence of the mean stress. Accordingly, the mean stress is adopted to describe void growth here. The influence of the mean stress is introduced by the terminology of the non-dimensional stress triaxiality η defined as the ratio of the mean stress to the equivalent stress. The equation of the stress triaxiality is further extended to include a cut-off value of $-1/3$ for the stress triaxiality

below which ductile fracture will never occur (Bao and Wierzbicki, 2005). The extended equation then has in a form of

$$D_g = D_g(\langle 1+3\eta\rangle) \quad \langle x\rangle = \begin{cases} x & \text{when} \quad x \geqslant 0 \\ 0 & \text{when} \quad x < 0 \end{cases} \tag{2}$$

2.1.3. Coalescence of voids

Coalescence of voids is the final stage of ductile fracture. Mechanisms of coalescence are then correlated with the macroscopic fracture surface. As shown in Fig. 1, two coalescence mechanisms were reported using model materials (Weck and Wilkinson, 2008): the necking of the ligaments between voids caused by the highest principal stress; shear-linking up of voids along the direction of the maximal shear stress. These two mechanisms were also observed from the SEM fractographies of upsetting tests, shear tests, tensile tests of smooth and notched round bars (Bao and Wierzbicki, 2004; Li et al., 2011). The necking of the ligaments between voids is referred as dimple-dominant fracture while the linking up of voids is named as shear fracture (Li et al., 2011). The dimple-dominant fracture, however, was not found in sheet metals (Ghosh, 1976). Therefore shear fracture is assumed for sheet metals. A number of models were proposed to describe shear fracture (McClintock et al., 1966; Ghosh, 1976; Bressan and Williams, 1983; Xue, 2008; Bai and Wierzbicki, 2010; Li et al., 2010). Since shear fracture is caused by the maximal shear stress, the void coalescence is modeled by the maximal shear stress normalized by the equivalent stress in a form of

$$D_c = D_c\left(\frac{\tau_{\max}}{\bar{\sigma}}\right) \tag{3}$$

2.2. A new ductile fracture criterion

Based on the microscopic analysis of ductile fracture, a new ductile fracture criterion is proposed with the selected models to describe mechanisms of nucleation, growth and coalescence of voids as mentioned above in a form of

$$\left(\frac{2\tau_{\max}}{\bar{\sigma}}\right)^{C_1}\left(\frac{\langle 1+3\eta\rangle}{2}\right)^{C_2}\bar{\varepsilon}_f = C_3 \quad \langle x\rangle = \begin{cases} x & \text{when} \quad x \geqslant 0 \\ 0 & \text{when} \quad x < 0 \end{cases} \tag{4}$$

which is simply multiplication of the three damage accumulating models for nucleation, growth and shear coalescence of voids with the exponents C_1 and C_2. In this new ductile fracture criterion, the void nucleation is assumed to be proportional to the equivalent plastic strain $\bar{\varepsilon}$, the void growth is represented by a function of the stress triaxiality as $1+3\eta$, and the coalescence of voids is described by the normalized maximal shear stress denoted as $\tau_{\max}/\bar{\sigma}$. Two exponents C_1 and C_2 are introduced to both the normalized maximal shear stress term and the stress triaxiality term to modulate the different effect of nucleation, growth and coalescence of voids on ductile fracture.

The material constant C_3 is equal to the equivalent plastic strain to fracture $\bar{\varepsilon}_{t0}$ in the uniaxial tension since a proper constant of 2 in the denominator is selected for the terms of $\tau_{\max}/\bar{\sigma}$ and $1+3\eta$ in the new model of Eq. (4). This constant could be replaced by 3 for the term of the stress triaxiality as $(1+3\eta)/3$ such that the material constant of C_3 is equal to the equivalent plastic strain to fracture $\bar{\varepsilon}_{b0}$ in the balanced biaxial tension. This was recommended by Dr. H. Aretz through personal communication. The huge benefit of the constant of 3 over that of 2 is that the fracture strain can be readily used from the bulge-test. It is more convenient for the calibration of material constants due to the fact that necking is less severe in the balanced biaxial tension than in the uniaxial tension. Sometimes, fracture in the balanced biaxial tension is observed even without preceding necking. Tremendous efforts are saved due to omission of complicated inverse, digital image correlation (DIC) and hybrid experimental-numerical methods (Bao and Wierzbicki, 2004; Dunand and Mohr, 2010) to determine the equivalent plastic strain to fracture in the uniaxial tension.

When the loading path and plastic deformation are not proportional, but localized non-linear, it is better to modify the proposed model into an integral form like other criteria as below:

$$\frac{1}{C_3}\int_0^{\bar{\varepsilon}_f}\left(\frac{2\tau_{\max}}{\bar{\sigma}}\right)^{C_1}\left(\frac{\langle 1+3\eta\rangle}{2}\right)^{C_2} d\bar{\varepsilon} = D(\bar{\varepsilon})$$
$$\langle x\rangle = \begin{cases} x & \text{when} \quad x \geqslant 0 \\ 0 & \text{when} \quad x < 0 \end{cases} \tag{5}$$

Fracture initiates when the accumulated damage $D(\bar{\varepsilon})$ reaches to unity. The integral form above can be easily implemented into numerical analysis to describe ductile fracture in complex strain paths. It may be justified that the material constants C_1 and C_2 should be varied with deformation and should not be constant during deformation. However, it might be acceptable to assume that the material constants are unchangeable for simplicity of evaluation like other ductile fracture criteria in Appendix.

2.3. Parametric study

Material constants in the new ductile fracture criterion modulate the effect of nucleation, growth and shear coalescence of voids on the plastic strain to fracture. Their effect on FFLDs will be

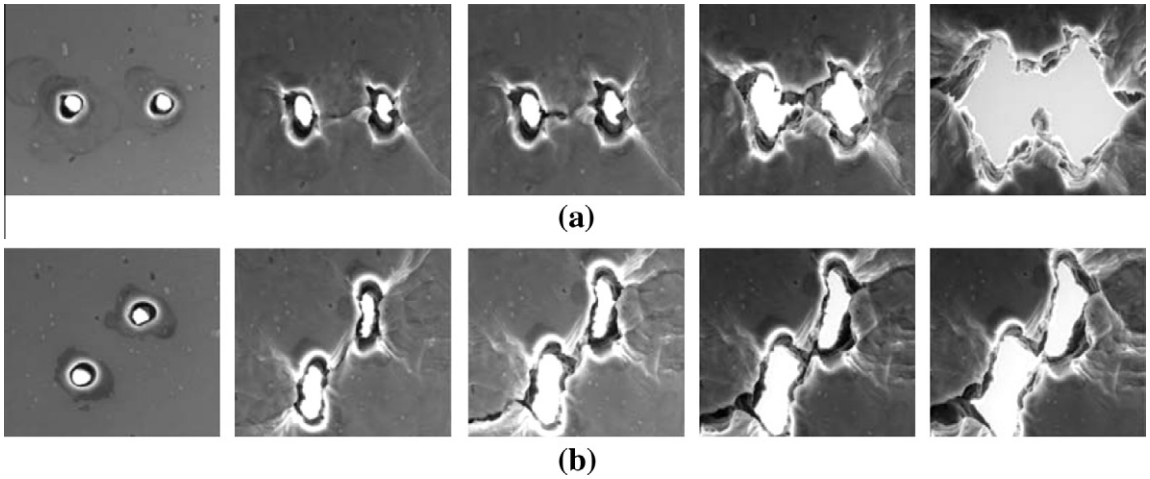

Fig. 1. Two kinds of mechanisms for coalescence of voids: (a) necking of inter-void ligaments; (b) shear-linking up of voids. [After Weck and Wilkinson.]

investigated to provide a deep understanding of the new ductile fracture criterion.

2.3.1. Effect of the material constant C_1

The material constant C_1 modulates effect of the normalized maximal shear stress on shear coalescence of voids during plastic deformation. As C_1 becomes large, influence of the maximal shear stress on ductile fracture increases and the fracture strain is reduced. Effects of C_1 are presented in the space of the major and minor strain $(\varepsilon_2, \varepsilon_1)$ in Fig. 2. The material constant C_1 simultaneously adjusts the ratio of the equivalent plastic strain to fracture in the uniaxial tension to that both in the pure shear and plane strain. This ratio increases with the material constant C_1. This makes sense since the normalized maximal shear stress increases from 1/2 in the uniaxial compression to a maximum in the pure shear, then decreases to 1/2 in the uniaxial tension, rises again until it reaches another maximum in the plane strain and then return to 1/2 again in the balanced biaxial tension, as presented in Fig. 3.

2.3.2. Effect of the material constant C_2

The material constant C_2 modulates effect of the stress triaxiality on growth of voids. As presented in Fig. 3, the normalized maximal shear stress is symmetric with respect to $\beta = -0.5$ in the uniaxial tension while the stress triaxiality monotonically increases from $-1/3$ in the uniaxial compression to 2/3 in the balanced biaxial tension. Without the effect of the stress triaxiality, the equivalent plastic strain to fracture will be identical for the same normalized maximal shear stress both in plane strain and pure shear, as proved in Eq. (4) when $C_2 = 0$. As analyzed in Section 2.1.2, high mean stress accelerates void growth while negative mean stress suppresses void growth, thereby delaying fracture. The equivalent plastic strain to fracture is lower at higher stress triaxiality than that at the low stress triaxiality even though the normalized maximal shear stress is equal in both plane strain and pure shear. This effect of the stress triaxiality is correctly modeled by the new ductile fracture criterion as presented in Fig. 4.

2.3.3. Effect of the material constant C_3

The role of the material constant C_3 is quite simple compared with roles of C_1 and C_2. It just varies the magnitude of FFLDs with no influence on the shape as presented in Fig. 5. As explained in Section 2.2, the new ductile fracture criterion is carefully modeled by adding proper constant values to simplify the form of the new ductile fracture criterion in the uniaxial tension. The material constant C_3 is endowed a special meaning in the new ductile fracture criterion: the equivalent plastic strain to fracture in the uniaxial tension. This special meaning is useful in calculation of material constants as presented in Eq. (6) in Section 2.4.

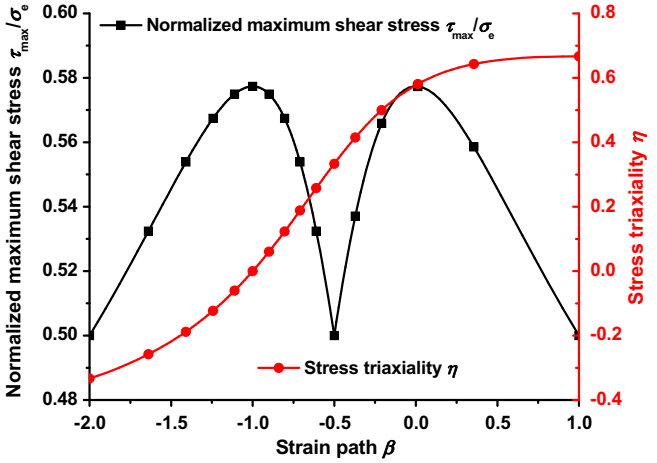

Fig. 3. Variation of the normalized maximal shear stress and the stress triaxiality depending on the strain path.

2.4. Calculation of material constants

There are three material constants in the new ductile fracture criterion: C_1, C_2 and C_3. These material constants should be calculated by at least three experimental data points. The simple tests to be carried out for sheet metals include the uniaxial tensile test, the plane strain test, the pure shear test and the hydraulic bulge test (balanced biaxial tensile test). The new ductile fracture criterion is reduced to a simple equation in each condition. For the uniaxial tension with $\tau_{max}/\bar{\sigma} = 1/2$ and $\eta = 1/3$, the material constant C_3 is easily obtained as:

$$C_3 = \bar{\varepsilon}_{t0} \tag{6}$$

In the plane strain condition with $\tau_{max}/\bar{\sigma} = \eta = 1/\sqrt{3}$, Eq. (4) is reduced to a form of

$$\left(\frac{2}{\sqrt{3}}\right)^{C_1}\left(\frac{1+\sqrt{3}}{2}\right)^{C_2}\bar{\varepsilon}_{p0} = C_3 \tag{7}$$

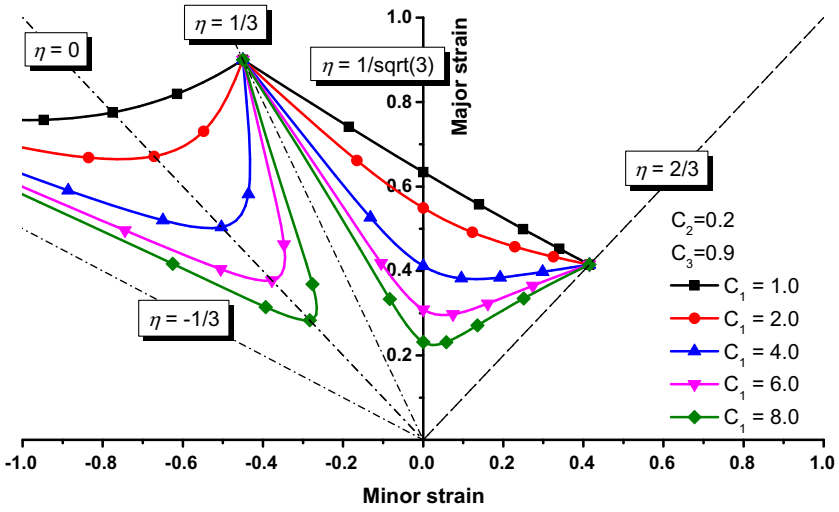

Fig. 2. Effect of material constants C_1 in the new ductile fracture criterion on the formability prediction in the space of $(\varepsilon_2, \varepsilon_1)$.

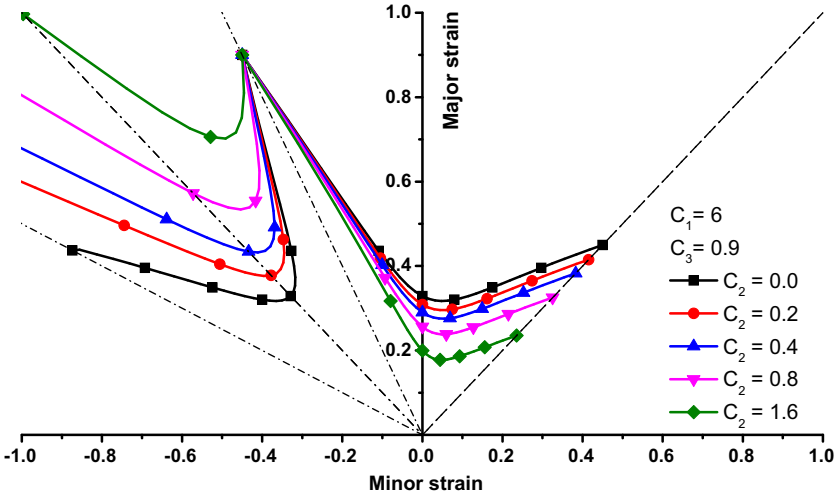

Fig. 4. Effect of material constants C_2 in the new ductile fracture criterion on the formability prediction in the space of $(\varepsilon_2, \varepsilon_1)$.

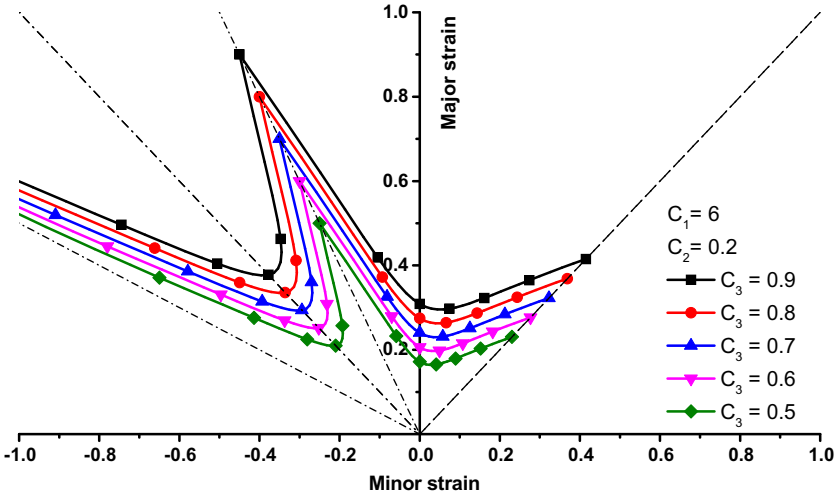

Fig. 5. Effect of material constants C_3 in the new ductile fracture criterion on the formability prediction in the space of $(\varepsilon_2, \varepsilon_1)$.

In the balanced biaxial tension with $\tau_{max}/\bar{\sigma} = 1/2$ and $\eta = 2/3$, the new ductile fracture criterion has a form of

$$\left(\frac{3}{2}\right)^{C_2} \bar{\varepsilon}_{b0} = C_3 \tag{8}$$

In the pure shear condition with $\tau_{max}/\bar{\sigma} = 1/\sqrt{3}$ and $\eta = 0$, the new ductile fracture criterion has a form of

$$\left(\frac{2}{\sqrt{3}}\right)^{C_1} \left(\frac{1}{2}\right)^{C_2} \bar{\varepsilon}_{s0} = C_3 \tag{9}$$

Any three equations of Eqs. (6)–(9) are sufficient to calculate the material constants C_1, C_2 and C_3 in the new ductile fracture criterion. These conditions, however, are ideal cases which cannot be achieved in practical experiments due to necking and other factors. Moreover, more experimental data points are preferred to construct a fracture locus with high accuracy. Therefore, an optimization method is suggested to calculate these material constants.

For the material constant C_2, it should be a positive value. That is because the material constant $C_2$is calculated from Eqs. (7) and (9) as below:

$$C_2 = \frac{\log(\bar{\varepsilon}_{s0}) - \log(\bar{\varepsilon}_{p0})}{\log(1+\sqrt{3})} \tag{10}$$

From the equation above, a positive value of C_2 is guaranteed if $\bar{\varepsilon}_{s0} > \bar{\varepsilon}_{p0}$ which is true since the normalized maximal shear stress is $1/\sqrt{3}$ for both pure shear and plane strain but the lower triaxiality in pure shear raises the equivalent plastic strain to fracture than that in plane strain tension. The material constant C_3 is equal to the equivalent plastic strain to fracture as presented in Eq. (6).

3. Application to the FFLD prediction of DP780

3.1. Experiments

The material used is an advanced high strength steel sheet of DP780 whose thickness is 1.0 mm. DP780 is observed to fail with

Table 1
Mechanical properties obtained from experiments.

K [MPa]	ε_0	n	$\bar{\varepsilon}_{t0}$	$\bar{\varepsilon}_{p0}$	$\bar{\varepsilon}_{b0}$
1429	0.002	0.179	0.28	0.21	0.84

unnoticeable necking whose region is narrow compared to lower strength steels from the SEM image of the fracture surface. Uniaxial tensile tests were conducted to obtain the true stress–true strain curve of DP780. Then true stress–true strain relation is interpolated following the Swift strain hardening curve of $\bar{\sigma} = K(\varepsilon_0 + \bar{\varepsilon})^n$. The material constants in the Swift model are summarized in Table 1. Punch-stretch tests were conducted to construct the FFLD experimentally. Circle grids with a diameter of 5 mm were used to calculate the limit strain from the deformation of the circles after tests. Different sample geometries and lubrication conditions were employed to generate all possible states of stress and strain (Kim et al., 2011; Huh et al., 1998) from the uniaxial tension to the balanced biaxial tension. Strain paths from the uniaxial tension to the plane strain tension are obtained using arc-shaped specimens, which are specially designed to prevent failure from occurring at the blank holder region and to induce the failure near the center region. Teflon and Plasticine were used as lubricants for this set of specimens. Another set of specimens are square plates with 200 mm × 200 mm. Various strain paths are attained using different lubrication conditions such as dry (D), Teflon (T), Teflon + Vaseline (T + V) and Teflon + Plasticine (T + P). The punch-stretch test was performed with a universal testing machine (UTM) equipped with a blank holder frame. The punch forming speed was 20 mm/min. The specimens of DP780 tested are shown in Fig. 6. It is noted from the figure that the fracture takes place in the shear direction through the thickness especially in the biaxial tension states. The fracture strains are approximated using the CGA method by comparing the dimensions of grids etched on specimens before and after deformation (Kim et al., 2011) as presented in Fig. 7.

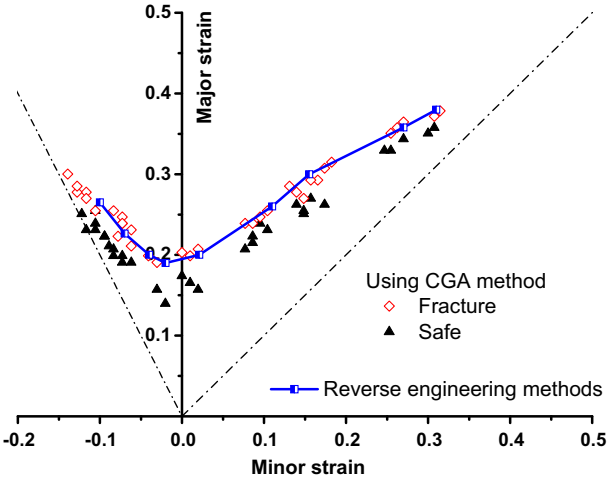

Fig. 7. Comparison of FFLDs from the CGA method with the one from the reverse engineering method.

3.2. FFLD from the reverse engineering method

The reverse engineering method is normally utilized to measure fracture strains (Bao and Wierzbicki, 2004; Wierzbicki et al., 2005). Here this method is also adopted to construct the FFLD of DP780. The limit dome heights (LDH) are measured from fractured specimens in Fig. 6 and summarized in Table 2. Simulations are carried out to numerically obtain the evolution of major and minor strains with respect to the deformation for nine tests. The equivalent coefficients of friction in numerical analysis are correlated with experiments using the square-shaped specimens based on the assumption that the strain states at the fracture initiation point in simulation are similar to those from experiments as presented in Fig. 8. Using the correlated coefficients of friction, the evolution of major and minor strains are obtained from numerical analysis as presented in Fig. 9 for the square-shaped specimens lubricated by T + V. The major and minor strains at fracture are then easily obtained at the fracture stroke or the LDH. With this method, nine pairs of fracture strains are measured and compared to those using the CGA method in Fig. 7. Both methods generate close results. This is because DP780 fails with negligible necking, which can be proved by the SEM image of the fracture surface for the uniaxial tensile test specimen as illustrated in Fig. 10. This observation is quite useful because the fracture strain of this metal can be measured directly using the technique of CGA since the deformation in a circle grid is almost homogeneous. Moreover, slant fracture surfaces are observed, which implies that shear fracture takes place. Therefore, the shear controlled ductile fracture model of Eq. (4) is quite suitable to describe the fracture behavior of DP780. From the distribution of fractured microscopic voids in the center and near the sheet surface in Fig. 10, the coalescence of voids is closely related with the direction of the maximum shear stress. This microscopic observation also validates the applicability of the new model to this material.

3.3. Comparison of predicted FFLDs to experimental results

Since FFLDs measured show a good coincidence between the results from CGA and reverse engineering methods, the FFLD from

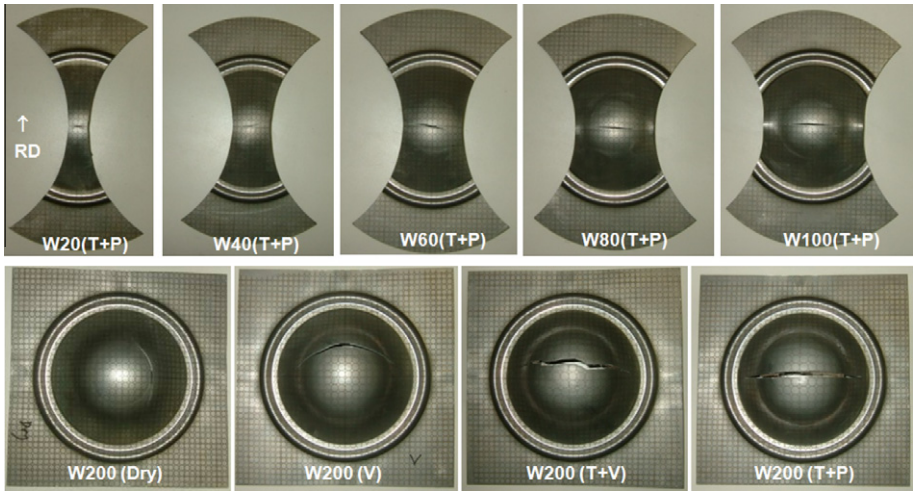

Fig. 6. Deformed shapes of specimens of DP780 obtained from punch-stretch tests.

Table 2
LDHs measured from fractured specimens of DP780 [unit: mm].

20(TP)	40(TP)	60(TP)	80(TP)	100(TP)	200(D)	200(T)	200(TV)	200(TP)
18.84	25.05	26.85	28.37	27.55	28.28	33.79	35.88	36.60

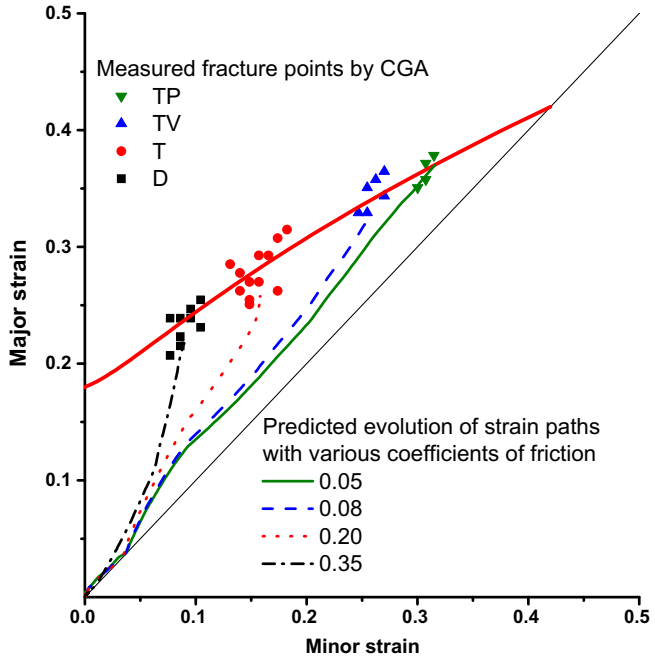

Fig. 8. Correlation of the equivalent friction coefficients in simulation to the one in experiments.

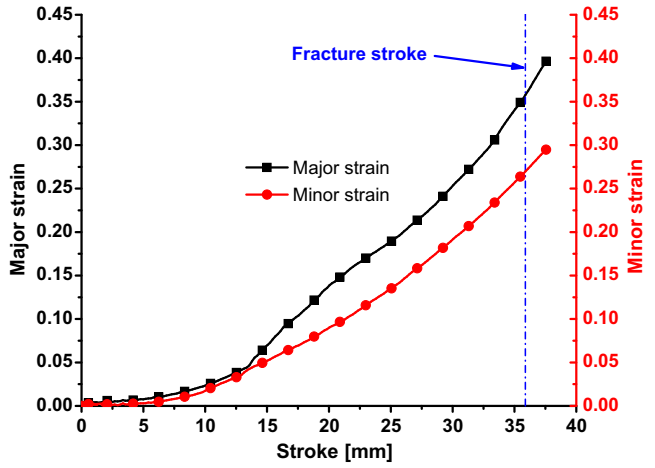

Fig. 9. Fracture strains by the reverse engineering method for the square-shaped specimen lubricated with Teflon and Vaseline.

the CGA method is utilized for the evaluation of the new criterion. From the experimental FFLD, the fracture major and minor strains are approximated in the uniaxial tension, plane strain and balanced biaxial tension conditions. The corresponding von Mises equivalent plastic strains to fracture are calculated and summarized in Table 1. Material constants C_1, C_2 and C_3 in the new ductile fracture criterion are calculated with Eqs. (6)–(8) after careful experiments of the uniaxial, the plane strain and the balanced biaxial tensile tests as mentioned above. These material constants are utilized to predict FFLDs with the new ductile fracture criterion. Predicted FFLDs are compared with experimental results in Fig. 11 for DP780. The comparison clearly demonstrates that FFLDs constructed by the new criterion are close to the experimental data points from the uniaxial tension to the balanced biaxial tension.

4. Application to predict the fracture locus of Al 2024-T351

4.1. Experimental results

Bao (2003) carried out fifteen different tests on Al 2024-T351 covering a wide range of the stress triaxiality from −0.3 to 1.0 which provide a schematic clue to the effect of the stress triaxiality on the equivalent plastic strain to fracture. The equivalent plastic strains to fracture of these tests were presented with the corresponding stress triaxiality η and the Lode angle parameter $\bar{\theta}$ by Wierzbicki et al. (2005) and Bai and Wierzbicki (2010) with slight difference. The stress triaxiality and the Lode angle parameter were given as the average values predicted by numerical analysis of experiments since these two parameters were not constant during the entire deformation. The Lode angle θ is calculated by to the definition of the Lode angle parameter as below:

$$\theta = \frac{\pi}{6}(1-\bar{\theta}) \tag{11}$$

The principal stresses can be expresses in terms of $(\eta, \theta, \bar{\sigma})$ as follows:

$$\sigma_1 = \sigma_m + s_1 = \sigma_m + \frac{2}{3}\bar{\sigma}\cos\theta = \left(\eta + \frac{2}{3}\cos\theta\right)\bar{\sigma} \tag{12}$$

$$\sigma_2 = \sigma_m + s_2 = \sigma_m + \frac{2}{3}\bar{\sigma}\cos\left(\frac{2}{3}\pi - \theta\right) = \left(\eta + \frac{2}{3}\cos\left(\frac{2}{3}\pi - \theta\right)\right)\bar{\sigma} \tag{13}$$

$$\sigma_3 = \sigma_m + s_3 = \sigma_m + \frac{2}{3}\bar{\sigma}\cos\left(\frac{4}{3}\pi - \theta\right) = \left(\eta + \frac{2}{3}\cos\left(\frac{4}{3}\pi - \theta\right)\right)\bar{\sigma} \tag{14}$$

Readers are recommended to refer to Bai and Wierzbicki (2010) for the detailed deriving processes of Eqs. (12)–(14). The normalized maximal shear stress is obtained in terms of θ as below:

$$\frac{\tau_{\max}}{\bar{\sigma}} = \frac{\sigma_1 - \sigma_3}{2\bar{\sigma}} = \frac{1}{3}\left(\cos\theta - \cos\left(\frac{4}{3}\pi - \theta\right)\right) \tag{15}$$

The Lode angle θ and the normalized maximal shear stress $\tau_{\max}/\bar{\sigma}$ are then calculated from $\bar{\theta}$ of Bai and Wierzbicki (2010) with Eqs. (11) and (15) and presented with the corresponding $\bar{\varepsilon}_f$ and η in Table 3.

4.2. Comparison of predicted fracture loci to experimental results

Material constants in the new ductile fracture criterion are calculated by the optimization method using all experimental data points in Table 3. The new ductile fracture criterion is applied to construct the fracture locus of Al 2024-T351 as presented in Fig. 12 in the space of the stress triaxiality and the equivalent plastic strain to fracture. A constant cut-off value of the stress

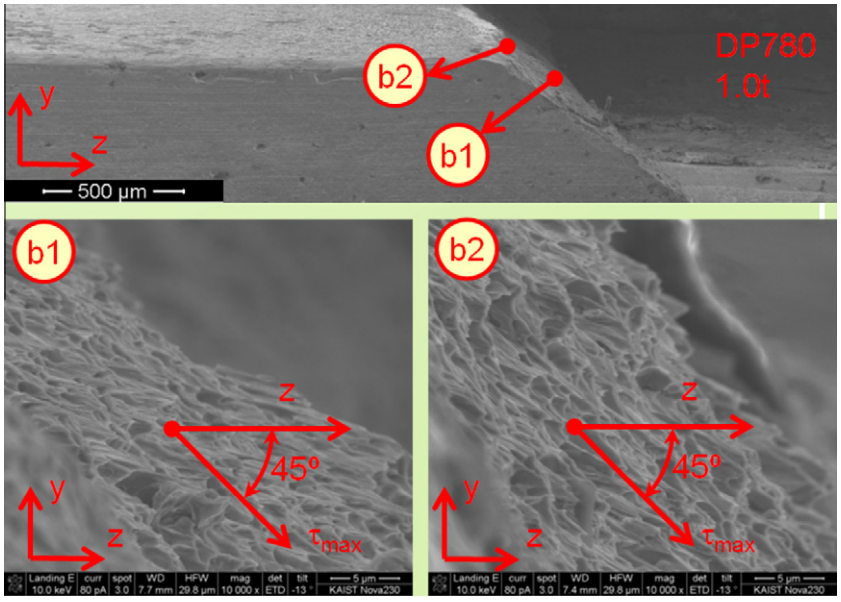

Fig. 10. SEM images of fractured surfaces.

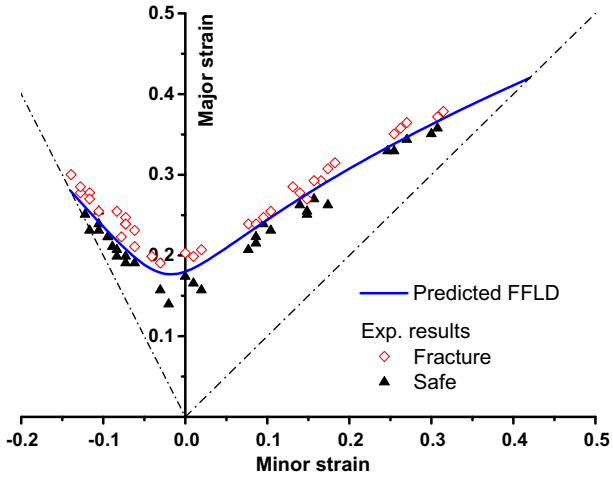

Fig. 11. Comparison of the predicted FFLD with experimental results. ($C_1 = 7.95$, $C_2 = -2.71$, $C_3 = 0.28$).

triaxiality is observed at $\eta = -1/3$ which is intentionally endowed in the new criterion as explained in Section 2.1.2. The importance of a cut-off value has been confirmed in high velocity impact simulation (Teng and Wierzbicki, 2006). There are two separate branches on the fracture locus. One branch is represented by $\sigma_3 = 0$ which constructs the equivalent plastic strain to fracture in the intermediate stress triaxiality $1/3 \leqslant \eta \leqslant 2/3$ from the uniaxial tension to the balanced biaxial tension. The other one is denoted as $\sigma_2 = 0$ which expresses the equivalent plastic strain to fracture in the low and negative stress triaxiality $-1/3 < \eta \leqslant 1/3$ from the uniaxial compression to the uniaxial tension. One additional branch of plane stress, $\sigma_1 = 0$, is not presented in Fig. 12 since the stress triaxiality is less than $-1/3$ below which fracture will never occur as postulated in the new ductile fracture criterion. The equivalent plastic strain to fracture in the uniaxial tension is higher than that in the balanced biaxial tension. It is also true that the equivalent plastic strain to fracture in the pure shear is greater than that in the plane strain tension. This condition is satisfactory to ensure a positive value of the material constant $C_2 = 0.22$.

Compared with experimental results, the fracture locus constructed by the new criterion is close to the experimental data points except the two experimental points with the test number of 2 and 3 in Table 3. This is due to coalescence of voids in the uniaxial tension of notched round bars in the high stress triaxility is caused by the necking of ligaments between voids which generates

Table 3
Experimental data points of Bao (2003) for Al 2024-T351. (After Bai and Wierzbicki, 2010.)

Test #	Specimens	$\bar{\varepsilon}_f$	η	θ	$\bar{\theta}$	$\tau_{max}/\bar{\sigma}$
1	Smooth round bar, tension	0.4687	0.4014	4.1888E−4	0.9992	0.5001
2	Round large notched bar, tension	0.2830	0.6264	4.1888E−4	0.9992	0.5001
3	Round small notched bar, tension	0.1665	0.9274	8.3776E−4	0.9984	0.5002
4	Flat-grooved, tension	0.2100	0.6030	0.4841	0.0754	0.5769
5	Cylinder ($d_0/h_0 = 0.5$), compression	0.4505	−0.2780	0.9537	−0.8215	0.5248
6	Cylinder ($d_0/h_0 = 0.8$), compression	0.3800	−0.2339	0.8801	−0.6809	0.5411
7	Cylinder ($d_0/h_0 = 1.0$), compression	0.3563	−0.2326	0.8793	−0.6794	0.5412
8	Cylinder ($d_0/h_0 = 1.5$), compression	0.3410	−0.2235	0.8650	−0.6521	0.5440
9	Round notched, compression	0.6217	−0.2476	0.8975	−0.7141	0.5375
10	Pure shear	0.2107	0.0124	0.5050	0.0355	0.5773
11	Shear tension	0.2613	0.1173	0.3466	0.3381	0.5683
12	Plate with a circular hole, tension	0.3099	0.3431	0.0178	0.9661	0.5051
13	Dog-bone specimen, tension	0.4798	0.3570	0.0428	0.9182	0.5119
14	Pipe, tension	0.3255	0.3557	0.0374	0.9286	0.5104
15	Solid square bar, tension	0.3551	0.3687	4.1888E−4	0.9992	0.5001

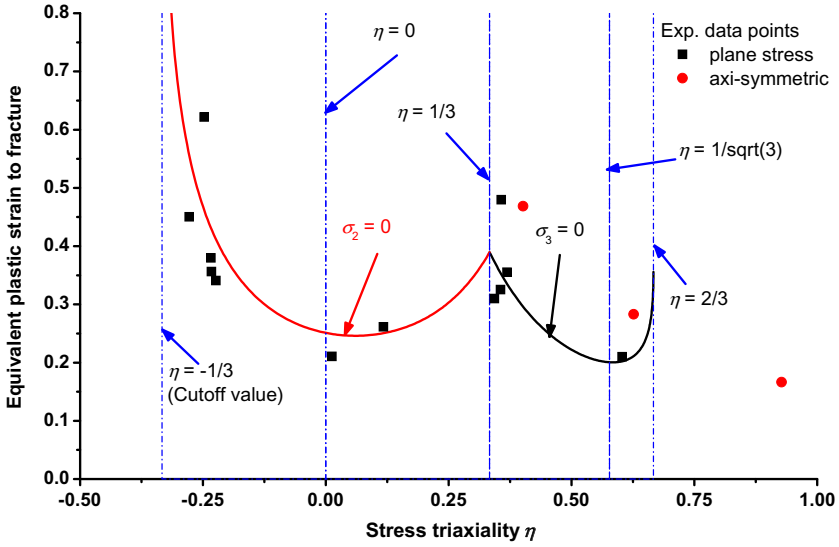

Fig. 12. Fracture locus constructed with the new ductile fracture criterion in the space of $(\eta, \bar{\varepsilon})$. ($C_1 = 4.13$, $C_2 = 0.22$, $C_3 = 0.39$).

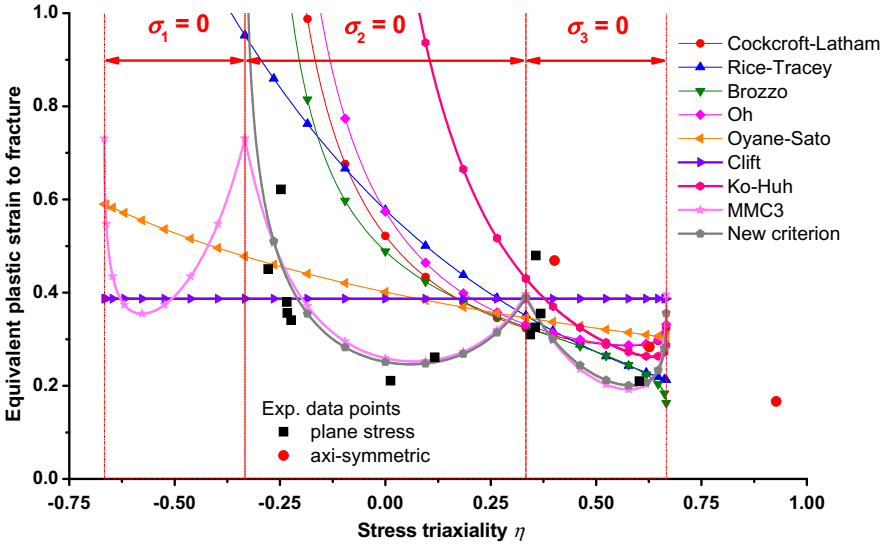

Fig. 13. Comparison of predicted fracture loci with experimental results in the space of $(\eta, \bar{\varepsilon})$.

dimple-dominated fracture surfaces rather than shear-linking up of voids as assumed in the new ductile fracture criterion of Eq. (4). The development of the new ductile fracture criterion, however, is based on the assumption of the shear-linking up of voids as presented in Section 2.1.3. Consequently, the application of the new ductile fracture is limited to the region where ductile fracture is caused by the shear-linking up of voids. Even though the boundary between dimple-dominated fracture and shear-linking up of voids is still not clear, the new ductile fracture criterion can be successfully applied to predict ductile fracture of sheet metals since shear-linking up of voids is the dominant mechanism of void coalescence in ductile fracture of sheet metals due to the relatively low triaxiality achieved in plane stress conditions.

For the purpose of comparison, material constants of another eight criteria in Appendix are calibrated using the same optimization method with all experimental data points. Fracture loci constructed by these ductile fracture criteria are compared to that predicted by the new criterion as illustrated in Fig. 13. All other criteria except the MMC3 criterion cannot predict the equivalent plastic strain to fracture in a wide stress state from the uniaxial compression ($\eta = -1/3$) to the balanced biaxial tension ($\eta = 2/3$). For the MMC3 criterion, a similar fracture locus is constructed compared to the new criterion when the stress triaxiality ranges between $-1/3$ to $2/3$. The essential difference between the MMC3 and the new criteria is that the new criterion assumes that fracture will never take place from the balanced biaxial compression ($\eta = -2/3$) to the uniaxial compression ($\eta = -1/3$) while fracture is possible for the MMC3 model in these stress states.

5. Conclusions

A ductile fracture criterion is newly proposed for prediction of FFLDs with efficient procedure to obtain the material constants in the criterion. The criterion is constructed with consideration of damage accumulation induced by nucleation, growth and shear coalescence of voids. These three processes are described as functions of the equivalent plastic strain, the stress triaxiality, and the normalized maximal shear stress to be multiplied to represent a fracture model. The model endows a cut-off value of $-1/3$ for the stress triaxiality for appropriate application to ductile materials.

The new ductile fracture is successfully applied to predict the FFLD of DP780 with high accuracy from the uniaxial tension to the balanced biaxial tension. The equivalent plastic strain to fracture in the low and negative triaxiality can also be properly estimated as validated by the constructed fracture locus of Al 2024-T351 in the space of $(\eta, \bar{\varepsilon})$. Comparison of the predicted fracture locus to those constructed by other fracture criteria also demonstrates the high accuracy of the new ductile fracture criterion. Ductile fracture of sheet metals can be correctly predicted by the new ductile fracture criterion based on the mechanism of shear-linking up of voids in a wide stress triaxiality ranging from $-1/3$ to $2/3$.

Appendix A

Forms of ductile fracture criteria used in this study are summarized as follows:

Cockcroft–Latham criterion (Cockcroft and Latham, 1968):

$$\int_0^{\bar{\varepsilon}_f} \sigma_1 d\bar{\varepsilon} = C_4 \tag{A.1}$$

Rice–Tracey criterion (Rice and Tracey, 1969):

$$\int_0^{\bar{\varepsilon}_f} 0.283 \exp\left(\frac{3\sigma_m}{2\bar{\sigma}}\right) d\bar{\varepsilon} = C_5 \tag{A.2}$$

Brozzo criterion (Brozzo et al., 1972):

$$\int_0^{\bar{\varepsilon}_f} \frac{2\sigma_1}{3(\sigma_1 - \sigma_m)} d\bar{\varepsilon} = C_6 \tag{A.3}$$

Oh criterion (Oh et al., 1979):

$$\int_0^{\bar{\varepsilon}_f} \frac{\sigma_1}{\bar{\sigma}} d\bar{\varepsilon} = C_7 \tag{A.4}$$

Oyane–Sato criterion (Oyane et al., 1980):

$$\int_0^{\bar{\varepsilon}_f} \left(\frac{\sigma_m}{\bar{\sigma}} + C_8\right) d\bar{\varepsilon} = C_9 \tag{A.5}$$

Clift criterion (Clift et al., 1990):

$$\int_0^{\bar{\varepsilon}_f} \bar{\sigma} d\bar{\varepsilon} = C_{10} \tag{A.6}$$

Ko–Huh criterion (Ko et al., 2007):

$$\int_0^{\bar{\varepsilon}_f} \frac{\sigma_1}{\bar{\sigma}} \left\langle 1 + \frac{3\sigma_m}{\bar{\sigma}} \right\rangle d\bar{\varepsilon} = C_{11} \quad \langle x \rangle = \begin{cases} x & \text{when} \quad x \geqslant 0 \\ 0 & \text{when} \quad x < 0 \end{cases} \tag{A.7}$$

Three parameter modified Mohr–Coulomb criterion (MMC3) (Bai and Wierzbicki, 2010):

$$\bar{\varepsilon}_f = \left\{ \frac{K}{C_{13}} \left[C_{14} + \frac{\sqrt{3}}{2-\sqrt{3}} (1 - C_{14}) \left(\sec\left(\frac{\pi\bar{\theta}}{6}\right) - 1 \right) \right] \times \left[\sqrt{\frac{1 + C_{12}^2}{3}} \cos\left(\frac{\pi\bar{\theta}}{6}\right) + C_{12} \left(\eta + \frac{1}{3} \sin\left(\frac{\pi\bar{\theta}}{6}\right) \right) \right] \right\}^{-\frac{1}{n}} \tag{A.8}$$

References

Argon, A.S., Im, J., Safoglu, R., 1975. Cavity formation from inclusions in ductile fracture. Metallurgical Transactions 6A, 825–837.

Bai, Y., Wierzbicki, T., 2008. A new model of metal plasticity and fracture with pressure and Lode dependence. International Journal of Plasticity 24, 1071–1096.

Bai, Y., Wierzbicki, T., 2010. Application of extended Mohr–Coulomb criterion to ductile fracture. International Journal of Fracture 161, 1–20.

Bao, Y.B., 2003. Prediction of ductile crack formation in uncracked bodies. PhD Thesis, Massachusetts Institute of Technology.

Bao, Y.B., Wierzbicki, T., 2004. On fracture locus in the equivalent strain and stress triaxiality space. International Journal of Mechanical Science 46, 81–98.

Bao, Y.B., Wierzbicki, T., 2005. On cut-off value of negative triaxiality for fracture. Engineering Fracture Mechanics 72, 1049–1069.

Bressan, J.D., Williams, J.A., 1983. The use of a shear instability criterion to predict local necking in sheet metal deformation. International Journal of Mechanical Science 25, 155–168.

Brozzo, P., DeLuca, B., Rendina, R., 1972. A new method for the prediction of formability in metal sheets. In: Proceedings of the 7th Biennial Conference of the International Deep Drawing Research Group on Sheet Metal Forming and Formability.

Chen, J.S., Zhou, X.B., Chen, J., 2010. Sheet metal forming limit prediction based on plastic deformation energy. Journal of Materials Processing Technology 210, 315–322.

Clift, S.E., Hartley, P., Sturgess, C.E.N., Rowe, G.W., 1990. Fracture prediction in plastic deformation processes. International Journal of Mechanical Science 32, 1–17.

Cockcroft, M.G., Latham, D.J., 1968. Ductility and the workability of metals. Journal of the Institute of Metals 96, 33–39.

Dunand, M., Mohr, D., 2010. Hybrid experimental-numerical analysis of basic ductile fracture experiments for sheet metals. International Journal of Solids and Structures 47, 1130–1142.

Ghosh, A.K., 1976. A criterion for ductile fracture in sheets under biaxial loading. Metallurgical Transactions 7A, 523–533.

Goods, S.H., Brown, L.M., 1979. The nucleation of cavities by plastic deformation. Acta Metallurgica 27, 1–15.

Goodwin, G.M., 1968. Application of strain analysis to sheet metal forming problems in the press shop. SAE Technical Paper No. 680093.

Gurson, A.L., 1977. Continuum theory of ductile rupture by void nucleation and growth. Part I: Yield criteria and flow rules for porous ductile media. ASME Journal of Engineering Materials and Technology 99, 2–15.

Han, H.N., Kim, K.H., 2003. A ductile fracture criterion in sheet metal forming process. Journal of Materials Processing Technology 142, 231–238.

Hill, R., 1952. On discontinuous plastic states, with special reference to localized necking in thin sheets. Journal of the Mechanics and Physics of Solids 1, 19–30.

Hora, P., Tong, L., Reissner, J., 1996. A prediction method for ductile sheet metal failure in FE-simulation. In: Proceedings of the Numisheet'96 Conference, Dearborn, Michigan, USA, pp. 252–256.

Hosford, W.F., Caddell, R.M., 1983. Metal Forming: Mechanics and Metallurgy. Prentice Hall International Editions.

Huh, H., Lee, C.H., Chung, J.W., 1998. Identification of forming limits of sheet metals for automobile parts by asymmetric deep-drawing experiments. Journal of the Korean Society for Technology of Plasticity 7, 81–93.

Keeler, S.P., Backofen, W.A., 1963. Plastic instability and fracture in sheets stretched over rigid punches. Transactions of American Society for Metals 56, 25–48.

Kim, S.B., Huh, H., Bok, H.H., Moon, M.B., 2011. Forming limit diagram of auto-body steel sheets for high-speed sheet metal forming. Journal of Materials Processing Technology 211, 851–862.

Ko, Y.K., Lee, J.S., Huh, H., Kim, H.K., Park, S.-H., 2007. Prediction of fracture in hub-hole expanding process using a new ductile fracture criterion. Journal of Materials Processing Technology 187 (188), 358–362.

Li, Y.N., Luo, M., Gerlach, J., Wierzbicki, T., 2010. Prediction of shear-induced fracture in sheet metal forming. Journal of Materials Processing Technology 210, 1858–1869.

Li, H., Fu, M.W., Lu, J., Yang, H., 2011. Ductile fracture: experiments and computations. International Journal of Plasticity 27, 147–180.

Liu, H.S., Yang, Y.Y., Yu, Z.Q., Sun, Z.Z., Wang, Y.Z., 2009. The application of a ductile fracture criterion to the prediction of the forming limit of sheet metals. Journal of Materials Processing Technology 209, 5443–5447.

Lou, Y.S., Huh, H., Ko, Y.K., Ha, J.W., 2010a. Comparative study of the ductile fracture criteria on the prediction of FLDs for aluminum alloys. In: Proceedings of KSAE Spring Conference, Pusan, Korea, pp. 40–45.

Lou, Y.S., Kim, S.B., Ko, Y.K., Huh, H., 2010b. Application of ductile fracture criteria for the FLD prediction of steel sheets. In: Proceedings of KSTP Fall Conference, Jeju, Korea, pp. 298–303.

Marciniak, Z., Kuczynski, K., 1967. Limit strains in the processes of stretch-forming sheet metal. International Journal of Mechanical Science 9, 609–620.

Marciniak, Z., Kuczynski, K., Pokora, T., 1973. Influence of the plastic properties of a material on the forming limit diagram for sheet metal in tension. International Journal of Mechanical Science 15, 789–805.

McClintock, F.A., Kaplan, S.M., Berg, C.A., 1966. Ductile fracture by hole growth in shear bands. International Journal of Fracture Mechanics 2, 614–627.

McClintock, F.A., 1968. A criterion of ductile fracture by the growth of holes. ASME Journal of Applied Mechanics 35, 363–371.

Oh, S.I., Chen, C.C., Kobayashi, S., 1979. Ductile fracture in axisymmetric extrusion and drawing: Part 2, workability in extrusion and drawing. ASME Journal of Engineering for Industry 101, 36–44.

Oyane, M., Sato, T., Okimoto, K., Shima, S., 1980. Criteria for ductile fracture and their applications. Journal of Mechanical Working Technology 4, 65–81.

Ozturk, F., Lee, D., 2004. Analysis of forming limits using ductile fracture criteria. Journal of Materials Processing Technology 147, 397–404.

Rice, J.R., Tracey, D.M., 1969. On the ductile enlargement of voids in triaxial stress fields. Journal of the Mechanics and Physics of Solids 17, 201–217.

Stören, S., Rice, J.R., 1975. Localized necking in thin sheets. Journal of the Mechanics and Physics of Solids 23, 421–441.

Swift, H.W., 1952. Plastic instability under plane stress. Journal of the Mechanics and Physics of Solids 1, 1–19.

Takuda, H., Mori, K., Hatta, N., 1999a. The application of some criteria for ductile fracture to the prediction of the forming limit of sheet metals. Journal of Materials Processing Technology 95, 116–121.

Takuda, H., Mori, K., Fujimoto, H., Hatta, N., 1999b. Prediction of forming limit in bore-expanding of sheet metals using ductile fracture criterion. Journal of Materials Processing Technology 92 (93), 433–438.

Takuda, H., Mori, K., Takakura, N., Yamaguchi, K., 2000. Finite element analysis of limit strain in biaxial stretching of sheet metals allowing ductile fracture. International Journal of Mechanical Science 42, 785–798.

Teng, X., Wierzbicki, T., 2006. Evaluation of six fracture models in high velocity perforation. Engineering Fracture Mechanics 73, 1653–1678.

Tvergaard, V., Needleman, A., 1984. Analysis of the cup-cone fracture in a round tensile bar. Acta Metallurgica 32, 157–169.

Weck, A., Wilkinson, D., 2008. Experimental investigation of void coalescence in metallic sheets containing laser drilled holes. Acta Materialia 56, 1774–1784.

Wierzbicki, T., Bao, Y.B., Lee, Y.-W., Bai, Y.L., 2005. Calibration and evaluation of seven fracture models. International Journal of Mechanical Science 47, 719–743.

Xue, L., 2008. Constitutive modeling of void shearing effect in ductile fracture of porous materials. Engineering Fracture Mechanics 75, 3343–3366.

Zhu, X., Weinmann, K., Chandra, A., 2001. A unified bifurcation analysis of sheet metal forming limits. ASME Journal of Engineering Materials and Technology 123, 329–333.